Microwave-Exfoliated Graphite Oxide/Polycarbonate Composites
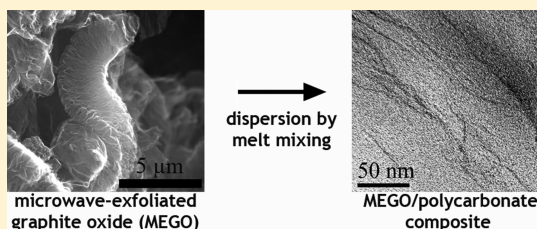
Jeffrey R. Potts,[†] Shanthi Murali,[†] Yanwu Zhu,[†] Xin Zhao,[‡,§] and Rodney S. Ruoff*,[†]

[†]Department of Mechanical Engineering and the Materials Science and Engineering Program, University of Texas at Austin, One University Station C2200, Austin, Texas 78712-0292, United States

[‡]State Key Laboratory for Modification of Chemical Fibers and Polymer Materials, College of Materials Science and Engineering, Donghua University, Shanghai 201620, P. R. China

ABSTRACT: We present the first report of polymer composites using microwave-exfoliated graphite oxide (MEGO) as filler, a high surface area carbon material that resembles graphene on a local scale. MEGO has a "wormlike" layered structure which can be sheared apart during melt mixing with a polymer host. In this study, we produced MEGO/polycarbonate (PC) composites at various loadings and evaluated their morphology and properties. Transmission electron microscopy and X-ray scattering studies suggested an exfoliated morphology, with wrinkled platelets of approximately 4–5 nm thickness evenly dispersed throughout the PC matrix.

microwave-exfoliated graphite oxide (MEGO) → dispersion by melt mixing → MEGO/polycarbonate composite

Frequency scans of composite melts using shear rheology showed an onset of frequency-independent terminal behavior around 2.1 wt %, suggesting an effective aspect ratio of nearly 50 for the dispersed platelets, in agreement with TEM analysis. The composites showed significant increases in electrical conductivity, with an onset of electrical percolation around 1.3 wt %, but only exhibited modest improvements in thermal conductivity. Long-term thermal annealing was performed to promote disorientation of the dispersed platelets, which further improved the electrical conductivity but had little effect on the thermal conductivity. Dynamic mechanical analysis showed reinforcement by MEGO; however, very little change in the glass transition temperature and in the thermal stability was observed in the composites versus neat PC.

1. INTRODUCTION

There is great interest in using graphene-based materials as fillers for polymer composites owing to the significant multifunctional property enhancements observed in these systems.[1,2] In recent studies, most graphene-based composite filler materials have been derived from graphite oxide (GO). GO can be produced by several different methods,[3] all of which generate a product that has a larger interlayer spacing than graphite (varying between 0.6 and 1.2 nm for GO, depending on humidity, compared to 0.34 nm for graphite) along with several oxygen-based functional groups decorating the basal planes and edges of the platelets (e.g., carboxylic acids, epoxides, alcohols)[3,4] in addition to the reported existence of strongly bound "oxidative debris".[5] These structural features act in tandem to facilitate the exfoliation of GO into individual graphene oxide sheets in water and, at lower concentrations, certain polar organic solvents. Once dispersed in a solvent, treatment with chemical reductants such as hydrazine or sodium borohydride can afford single-layer dispersions of reduced graphene oxide with the aid of electronic or steric stabilization.[6,7] It has also been shown that GO can be exfoliated and reduced via thermal shocking[8,9] (i.e., rapid heating under inert gas) or microwave treatment[10] to create loosely stacked, "wormlike" structures with a high specific surface area.

Solvent-exfoliated graphene oxide platelets (and associated chemically modified graphenes, such as reduced graphene oxide) as well as thermally exfoliated graphite oxide (TEGO) particles have been widely investigated as fillers for polymer composites.[1] In particular, TEGO can be dispersed into a polymer matrix via melt mixing operations which are highly compatible with industrial practice.[11–15] Microwave-exfoliated graphite oxide (MEGO) has a similar structure to TEGO,[9] which suggests MEGO may also disperse using melt mixing and might afford property enhancements comparable to TEGO.[13] However, the procedure for making MEGO is less time and energy intensive than the typical TEGO synthesis;[1,10] moreover, there are some differences in the reported physical properties of TEGO and MEGO, such as different C:O ratios (i.e., a generally lower C:O ratio for MEGO compared to TEGO) and different values of electrical conductivity (with TEGO generally being higher than MEGO), which could possibly affect dispersion or the final composite properties.[1] In light of these differences, we thus sought to investigate the property enhancements afforded by MEGO, using bisphenol A polycarbonate (PC) as a "model" matrix polymer, by using melt mixing to mix dry MEGO powder with PC to create well-dispersed MEGO/PC composites without the aid of solvents. Herein, we present the first report, to our knowledge, on the morphology and properties of a MEGO-filled polymer composite.

2. MATERIALS AND METHODS

2.1. Materials. SP-1 graphite (Bay Carbon), bisphenol A polycarbonate (M_w = 45 000 Da; Scientific Polymer), and all reagents used in the synthesis of GO were used as received.

2.2. Production of Composites. Graphite oxide (GO) was prepared via a modified Hummers method[16] and dried for 48 h under vacuum. The GO was loaded into a glass beaker, put into a domestic microwave oven (General Electric), and heated for ~20 s to cause rapid exfoliation and reduction of the material (the yield of MEGO relative to the starting amount of GO was ~20%). The black, fluffy powder was collected and compressed by hand to facilitate weighing and loading into the processing equipment. The polymer and MEGO powder were fed into a twin-screw DSM Xplore microcompounder with a mixing chamber volume of 5 mL. The composites were mixed with MEGO at the following weight percent loadings: 0.1, 0.5, 0.8, 1.3, 2.1, and 3.0 wt %, as confirmed by thermogravimetric analysis of the extrudates. Nominal loadings were higher than the values reported here; however, since MEGO has a low bulk density and some MEGO powder was lost during handling and particularly during the mixing step, actual loadings were found to be as much as 25% lower than the nominal values. For the microcompounding step, the melt mixing temperature was 250 °C, with a screw speed of 100 rpm and a residence time of 9 min. The extrudates were retrieved directly from the mixer and placed in a desicciator at room temperature for 24 h prior to molding. The dried extrudates were then pressed using a hydraulic hot press (Wabash) at 67 kN and 250 °C for 5 min and then cooled in the mold under pressure for 5 min (the mold temperature was below 100 °C after cooling), resulting in uniform films of ~0.3 mm thickness.

2.3. Characterization of MEGO. Elemental analysis by combustion was performed by Atlantic Microlabs in Norcross, GA. XPS analysis was performed using a Kratos AXIS Ultra DLD spectrometer (monochromated Al K emission at 1486.6 eV with an operating power of 150 W). A FEI Quanta-600 environmental scanning electron microscope (SEM) was used to image the morphology of the "wormlike" MEGO particles, which were pressed directly into carbon tape for imaging. A 30 kV accelerating voltage at ~10^{-6} Torr was used to image the dry powders. Determination of specific surface area using the Brunauer–Emmett–Teller (BET) equation[17] was carried out on a Quantachrome Instruments Nova 2000 using nitrogen as the adsorbent at 77 K.

2.4. Thermomechanical Analysis. The linear viscoelastic response of the composites was measured using dynamic mechanical analysis (DMA Q800, TA Instruments). Strips of composite of uniform width (~5 mm) were cut from the hot-pressed film (thickness of roughly 0.3 mm) using a razor blade. For fixed-frequency temperature scans, dynamic loading was applied in a tensile geometry at 1 Hz at 0.02% strain with a 0.01 N tensile force preload. A temperature ramp rate of 3 °C/min was used to obtain storage and loss modulus values as a function of temperature, and the tan delta peak was used to determine the glass transition temperature, T_g. Thermogravimetric analysis (TGA4000, Perkin-Elmer) was used to observe changes in nonoxidative thermal degradation behavior versus the neat polymer, using a ramp rate of 10 °C/min with N_2 as the sample purge gas.

2.5. Impact Testing. The impact strength of neat PC and the composites were measured according to ASTM D256. Samples were compression-molded into bars of specified dimensions ($6.4 \times 1.27 \times 0.32$ cm). Notched Izod impact tests were then performed at room temperature using a TMI Izod impact tester, with an impact velocity of 3.5 m/s.

2.6. Rheology. Rheological characterization of the composites was performed using a TA Instruments AR 2000EX rheometer. All samples were tested at 230 °C under flowing nitrogen. Approximately 0.75 g of the extrudates was loaded onto a 25 mm parallel plate fixture and subsequently squeezed to a disk of approximately 0.9–1 mm thickness for testing. For each sample loading tested, a dynamic strain sweep at 1 rad/s was performed to find the limit of linear viscoelasticity. The maximum strain before the drop in storage modulus (G') with increasing strain (before G' had decreased to ~95% of its limiting value) was recorded and used as the constant strain for the frequency sweep test. A frequency sweep at constant strain was then performed from 100 to 0.05 rad/s.

2.7. Composite Morphological Characterization. X-ray diffraction studies were performed using a Philips X-PERT diffractometer using Cu Kα radiation. A generating voltage of 40 kV and a current of 30 mA was used, with a 2 s dwell time. For transmission electron microscopy (TEM) imaging, the extrudates were microtomed (Leica Ultracut UCT, Reichert Inc.) at a direction perpendicular to the axis of extrusion to slices of approximately 75 nm thickness using an ultra45 diamond blade, then placed onto copper TEM grids (Ted Pella 300 mesh). The TEM images were acquired on a JEOL 2010F at 200 keV.

2.8. Electrical Conductivity Measurements and Annealing Treatment. Hot-pressed composite samples having ~0.3 mm thickness were cut into strips (roughly 3 mm wide and 5 mm long). A thin "skin" layer deficient in the microwave-exfoliated graphite oxide platelets was removed by oxygen plasma etching (Plasma-Preen II-862, Plasmatic Systems; 2 Torr of O_2, 3 min, 350 W) to reduce the contact resistance between the metal leads and sample tested. After etching, the small amounts of silver paste (SPI) were dropped onto the surface to lower the contact resistance of the probes, and the samples were then allowed to sit at room temperature for 24 h before measurement. Conductivity measurements were performed with a four-probe conductivity apparatus (Keithley 6514 electrometers and Keithley 6221 ac/dc source); the values were checked against a dc multimeter (Keithley 2410) with a threshold detection limit of ~0.2 GΩ. To calculate the conductivity, the thickness t of the sample was measured with calipers, and from the sheet resistance R_s measured by the four-probe measurement, the resistivity was calculated as $\rho = t R_s$ and then the conductivity was calculated as $\sigma = 1/\rho$ (units of S/m).

Long-term annealing treatments were performed on the composites in an attempt to randomize the orientations of the dispersed platelets with the goal of lowering the conductivity percolation threshold and raising the conductivity of the composites. For the annealing treatment, the samples were treated in a vacuum oven at 230 °C for 24 h. The conductivity measurements on the annealed samples were then performed identically to those samples which were not annealed.

2.9. Thermal Conductivity Measurements and Annealing Treatment. A symmetric, "guarded hot plate" thermal conductivity apparatus was assembled, and measurements were taken according to a previous report.[18] Briefly, two composite specimens of equivalent size (2.5 cm $\times 2.5$ cm $\times 0.3$ cm) were compression-molded at 250 °C and 67 kN for 3 min, then cooled inside the mold under pressure, and retrieved. After conditioning for 24 h, the faces of the specimens were coated in zinc oxide thermal grease, and a flexible polyimide heater (Minco, HK5951) of equivalent lateral dimensions to the specimens was sandwiched between them. Thermocouple contacts (of 0.08 mm diameter; Omega, CHAL-003) were placed on each face of the specimens. Two identical aluminum heat sinks were pressed on the outer faces of the specimens, and the whole apparatus was subsequently pressed together firmly with a spring clamp and covered with foil to provide radiation and convective shielding. A constant voltage and current was supplied (dc voltage source, Extech), and V and I were read from a display on the source (and independently measured using a multimeter) to calculate $Q = VI$ to obtain the heat flow, from which the thermal conductance and thus thermal conductivity could be calculated based on the sample geometry. Measurements at a given Q value were taken at regular intervals until the temperature readings were constant (typically 3–4 h). The accuracy of the setup was verified with neat samples of nylon-6 and polycarbonate by comparison against tabulated thermal conductivity values. For the annealing treatment, the samples were placed inside a mold (to maintain the sample geometry) and heated in a hot press (Fred S. Carver, Inc.) at 230 °C and ~1 kN for 14 h. The conductivity measurements on the annealed samples were then performed identically to those samples which were not annealed.

3. RESULTS AND DISCUSSION

3.1. Filler and Composite Morphology. Microwave-exfoliated graphite oxide has a fluffy, lightly stacked structure of wrinkled
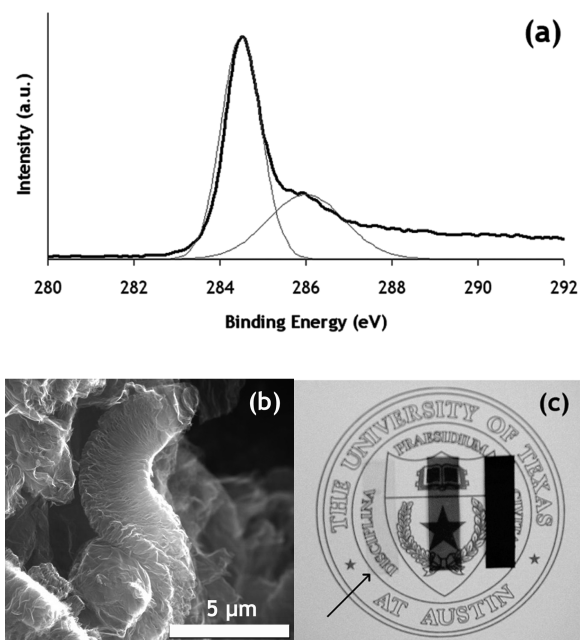
Figure 1. (a) C 1s XPS spectrum of MEGO with peak deconvolution shown. (b) SEM image of MEGO particles. (c) Image showing the loss of optical clarity in polycarbonate as a function of loading. From left to right: neat PC (barely visible; marked with arrow), 0.1 wt % MEGO/PC, and 0.5 wt % MEGO/PC. All samples shown are 0.27−0.30 mm thick.
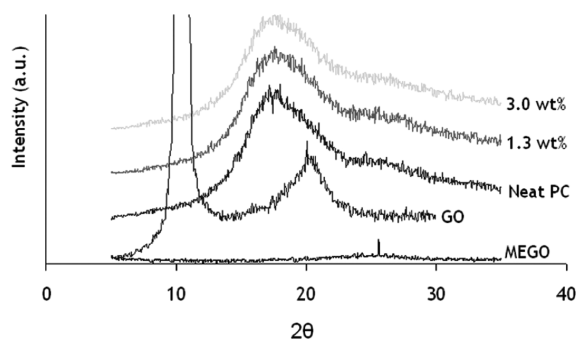

Figure 2. Normalized wide-angle X-ray scattering plots of GO, MEGO, neat PC, and MEGO/PC composites.

Figure 3. Representative TEM images of microtomed cross sections of 3.0 wt % MEGO/PC composites, showing the presence of crumpled, multilayered MEGO platelets dispersed throughout the PC matrix.

plots are shown for MEGO, neat PC, and MEGO/PC composites in Figure 2. The scattering intensity profile for MEGO is nearly featureless relative to GO, except for a slight, broad peak between 24° and 26° corresponding to a *d*-spacing of ∼0.35 nm. Since MEGO is largely exfoliated (relative to GO) before mixing into the PC matrix, it was expected that the composites would exhibit an exfoliated morphology according to X-ray scattering analysis. Figure 2 shows that no change in the scattering profile was observed even at the highest loadings of MEGO, suggesting that the composites have an exfoliated morphology and that no significant restacking occurs upon dispersion.

Microtomed cross sections of 3.0 wt % MEGO/PC composites were analyzed by TEM. The MEGO platelets show adequate contrast against the PC matrix to allow imaging without staining, although thinner platelets (particularly at lower magnifications) were difficult to clearly resolve. As evident from Figure 3, the platelets were largely multilayered and exhibited wrinkled conformations. The platelets were evenly dispersed throughout the matrix along with a low concentration of agglomerated platelets. Many of the platelets appear to be in contact in the images, suggesting that the MEGO particles have formed a percolating network at this loading, consistent with our electrical and rheological measurements.

Several images of the composite cross section were analyzed in attempt to quantify the dispersion of the MEGO/PC composite. On the basis of an analysis of platelet size in several TEM images, the platelets were estimated to have an average lateral dimension of 202 nm with an average thickness of roughly 4.5 nm, translating to an average platelet aspect ratio of ∼45. However, there is a possibility that few-layer or monolayer platelets—which may be "invisible" by TEM—were dispersed in the matrix, suggesting the actual average aspect ratio of the dispersed MEGO platelets may be higher than our estimation. Also, complications with analyzing dispersion from these two-dimensional projections could also affect this analysis.[19]

3.2. Rheological Properties. Melt rheological studies on the composites were performed to quantify dispersion.[20] For each loading tested, a strain sweep was first performed to identify the limit of linear viscoelasticity, followed by a constant-amplitude frequency sweep. The transition from liquidlike ($G' \sim \omega^2$ and $G'' \sim \omega$) to solidlike (G' and $G'' \sim \omega^0$) terminal behavior can provide a measure of the rheological percolation threshold for the composites[21] and can be used to calculate an effective aspect ratio (A_f) of the platelets, based on the idealized assumption of rigid, ellipsoidal tactoids.[22] Ren and co-workers[21,22] showed with a volume-filling calculation that the filler loading corresponding to the onset of percolation can be used to estimate the aspect ratio of

platelets as shown in Figure 1a. The particles appear "wormlike" at lower magnification due to the large *c*-axis expansion that results from the microwave treatment. As-prepared GO was determined to have a C:O ratio of 1.4:1, while MEGO was found to have a C:O ratio of 3.2:1 (approximately 2:1 according to XPS), roughly consistent with our earlier report on the synthesis and properties of MEGO.[10] XPS measurements indicated the presence of oxygen-based functional groups on the platelets, although in much lower concentration than GO. BET surface area measurements revealed a specific surface area of 432 m²/g for the platelets. Upon dispersion of MEGO into PC, the composites become black in color and thin films (∼0.3 mm) of composite become completely opaque at and above 0.5 wt % loading, as shown in Figure 1c.

Wide-angle X-ray scattering and TEM were used to probe the dispersion of MEGO in the composites. X-ray scattering
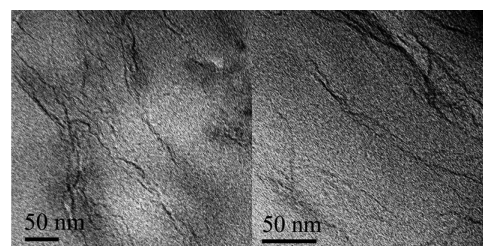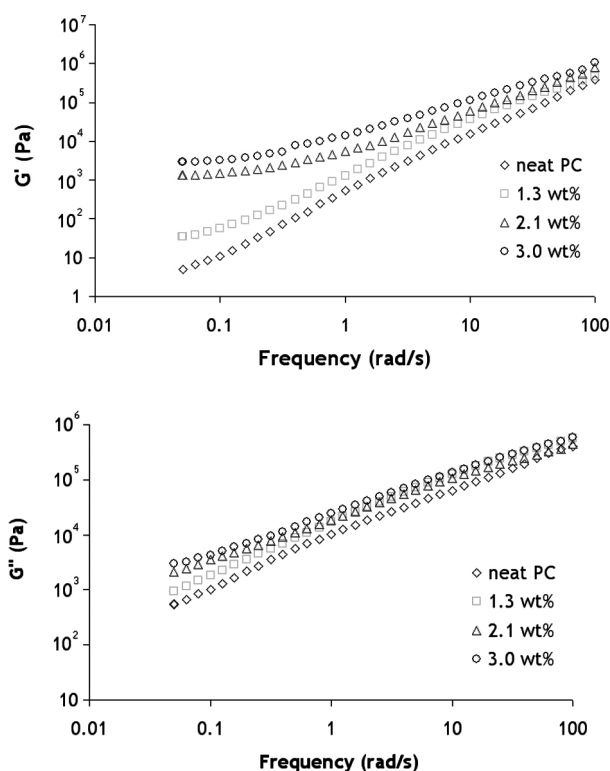
Figure 4. Frequency sweeps of MEGO/PC composite melts at 230 °C.

the platelets according to the equation[12]

$$A_f = \frac{3\phi_{sphere}}{2\phi_{perc}}$$

where ϕ_{sphere} is the percolation threshold for randomly dispersed spheres (=0.29) and ϕ_{perc} is the observed percolation threshold for this composite system. As shown in Figure 4, the onset of terminal behavior appears around 2.1 wt % (∼0.92 vol %, based on the density of graphite, 2.28 g/cm³), suggesting $A_f = 47$, in good agreement with the TEM observations—particularly considering that some few- or single-layer platelets may have been "invisible" by TEM, which would tend to decrease the A_f estimated from that analysis.

3.3. Mechanical Properties. The high aspect ratio and relatively high modulus of graphene-based materials[23,24] allows them to be the primary load-bearing component when dispersed into a polymer,[25] and thus significant reinforcement by graphene-based fillers has been previously reported.[26] In this study, dynamic mechanical analysis (DMA) was used to probe the mechanical properties of the composites; Figure 5 provides representative plots of the storage moduli (E') and tan delta of the composites as a function of temperature. E' was found to increase both below and above the glass transition temperature, T_g. Near room temperature, E' increased by over 30% versus neat PC at 3.0 wt %, while the rubbery plateau modulus increased by nearly 400% at the same loading. Additionally, the tan delta peak decreased in magnitude with loading but the breadth of the peaks remained constant.

For polymer composites which are transverse isotropic, the composite modulus can be approximated by analytical expressions based on Mori—Tanaka theory.[27,28] For this study, we compared the normalized storage moduli of the composites near room temperature to values predicted by Mori—Tanaka theory
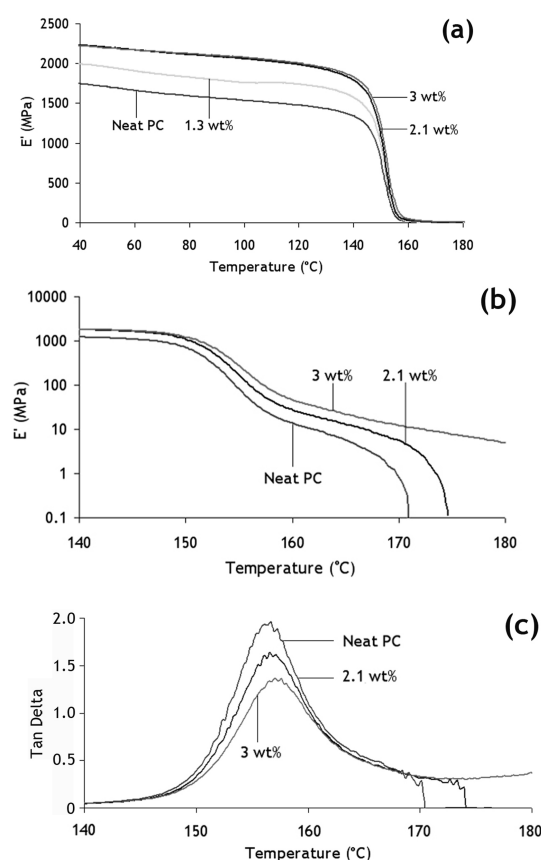

Figure 5. Plots of (a, b) storage modulus (E') and (c) tan delta versus temperature for various loadings of MEGO in PC.

to arrive at a rough estimate of the modulus of the MEGO platelets. The measured values of the composite moduli and aspect ratio, along with tabulated values for the Poisson's ratio, ν, of graphite and PC (equal to 0.06 and 0.37, respectively[12,29]), were used to extract a value for the effective platelet modulus according to the equation

$$E = \frac{E_m}{1 + \phi(-2\nu_m A_3 + (1 - \nu_m)A_4 + (1 + \nu_m)A_5 A)/2A}$$

where E is the composite modulus, E_m is the matrix elastic modulus, ϕ is the volume fraction of filler (converted from weight percent based on the density of graphite, ∼2.28 g/cm³), and the A_n are parameters that can be calculated from ϕ and ν following equations derived by Tandon and Weng.[28] Using the average platelet aspect ratio estimated from TEM analysis ($A_f = 45$), we calculated a value for the effective modulus of the MEGO platelets of ∼60 MPa based on the measured longitudinal moduli of the composites (Figure 6). This value is considerably lower than the measured value for "pristine" graphene[30] and also lower than the measured values for graphene oxide[23] and reduced graphene oxide,[24] which may be a consequence of defects in the platelet structure and also the wrinkled configuration of the platelets, in addition to the multilayer structure of the platelets.[31] In addition, the DMA measurements revealed very little increase in the T_g of the composites versus neat PC, consistent with other results on TEGO/PC composites.[11] In some other graphene-based composite systems, large increases in T_g (10—15 °C and, in some cases, higher) have been reported;[1,32] such large increases may be due to
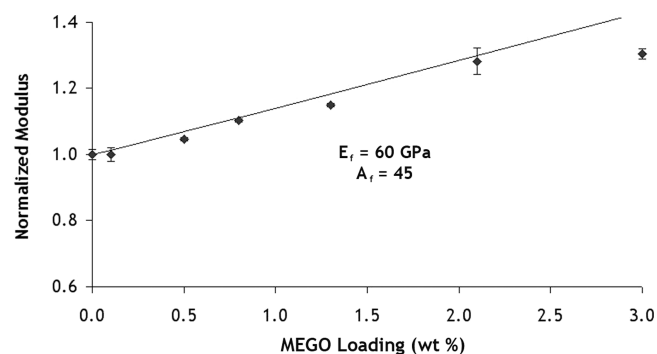
Figure 6. Comparison of experimental modulus data to calculations using Mori−Tanaka theory (using the aspect ratio, A_f, determined by TEM) provides an estimate of platelet modulus (E_f) of ∼60 GPa.

Table 1. Rheological and Dynamic Mechanical Properties and Impact Strengths of Neat PC and MEGO/PC Composites at Various Loadings

loading (wt %)	E' (1 Hz, 40 °C; GPa)	T_g (°C)	G' (0.05 rad/s, 230 °C; Pa)	Izod impact strength (J/m)
neat PC	1.74 ± 0.03	156.8 ± 0.2	5.0	700.6
0.1	1.74 ± 0.04	156.6 ± 0.2		
0.5	1.82 ± 0.01	157.0 ± 0.1	15.1	88.4
0.8	1.92 ± 0.01	156.7 ± 0.2		
1.3	2.07 ± 0.02	156.9 ± 0.1	44.4	41.4
2.1	2.23 ± 0.08	156.9 ± 0.1	1331	39.6
3.0	2.27 ± 0.03	157.4 ± 0.2	2921	20.0

comparatively better dispersion, resulting from more complete exfoliation of the platelets prior to mixing or resulting from the mixing step itself, or both.

The exceptional impact strength of PC is a major reason for its widespread application. Previously, the inclusion of layered silicate fillers into PC has been reported to compromise ductility and cause significant decreases in the Izod impact strength.[33,34] In this study, the composites exhibited brittle fracture at room temperature with significantly lower impact strength than neat PC, as shown in Table 1. Thus, while MEGO can be used to significantly improve the stiffness and conductivity properties of PC, it comes at the cost of impact strength.

3.4. Electrical Properties. A variety of graphene-based polymer composite systems have shown significant improvements in electrical conductivity versus the neat polymer matrix,[1] including PC-matrix composites.[11,13] In this study, we observed large improvements in the electrical conductivity as tested by a four-probe conductivity apparatus. For loadings below 1.3 wt %, the resistances of the composites were sufficiently high to be out of range of our test setup (∼0.2 GΩ). However, Figure 7a shows that a large increase in the conductivity of the composites began at 1.3 wt % (and increased further as the loading increased), thus suggesting an onset of conductivity percolation below that of rheological percolation. On the basis of the MEGO loading at the conductivity percolation threshold, $A_f = 74$, considerably higher than estimated from melt rheology or TEM. The onset of electrical percolation at a lower loading than rheological percolation has been established in other composite systems; however, our result stands in contrast to previous reports on TEGO-filled composites.[12,13] It should also be noted this electrical percolation
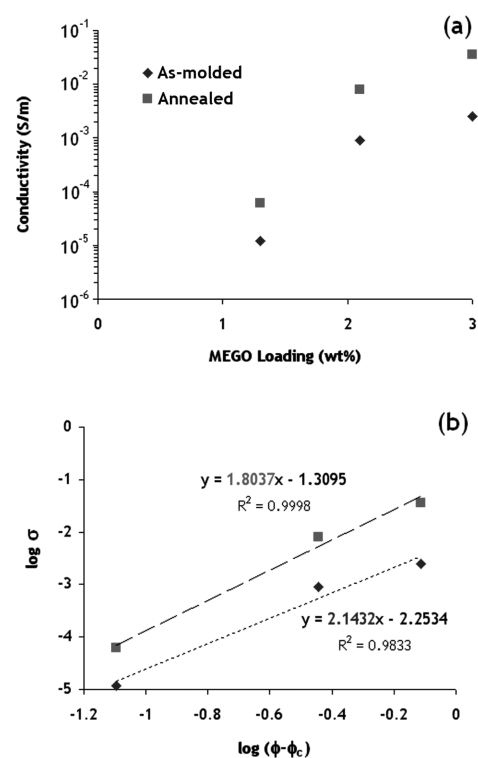

Figure 7. Measurements of electrical conductivity, σ, on neat PC and MEGO/PC composites; annealed samples were treated at 230 °C for 24 h. (a) Electrical conductivity data suggest electrical percolation around 1.3 wt %. At values below 1.3 wt %, the conductivity was too low to be determined by our laboratory setup, even after annealing. (b) Fitting of the conductivity power law above the percolation threshold allowed estimation of the critical exponent t, which was found to decrease on annealing.

threshold is comparable to or lower than what has been previously reported for TEGO/PC composites.[13,35]

It has been well-established in rheological studies that prolonged large-amplitude shear or other externally applied flow can suppress the terminal solidlike behavior in polymer composites by destroying a percolated network of filler particles, if one exists.[20,21] Thus, the conductivity percolation threshold and ultimate composite conductivity can be affected by such large strain deformations.[1] Previously, it has been reported that long-term annealing treatments under quiescent conditions can promote disorientation of dispersed, anisotropic fillers such as layered silicates[36] and, more recently, TEGO.[13] Prolonged thermal annealing of TEGO-reinforced polymer composites has been reported to improve electrical conductivity, by enhancing connectivity between filler particles (at sufficiently low concentrations).[13] The mechanisms for particle disorientation are not fully understood, but rheological measurements on layered silicate composites suggest the process may be non-Brownian (i.e., not dependent upon matrix viscosity or particle size) and has a power-law dependence on time.[36]

We thus sought to investigate whether long-term thermal annealing could further improve the conductivity of MEGO/PC composites under the presumption that the ∼0.3 mm thick samples hot pressed for conductivity measurements contain highly-aligned platelets as a consequence of the sample geometry. For their TEGO/PC composites ($M_w \sim 50$ kDa), Kim and co-workers[13] calculated a rotational relaxation time of rigid,
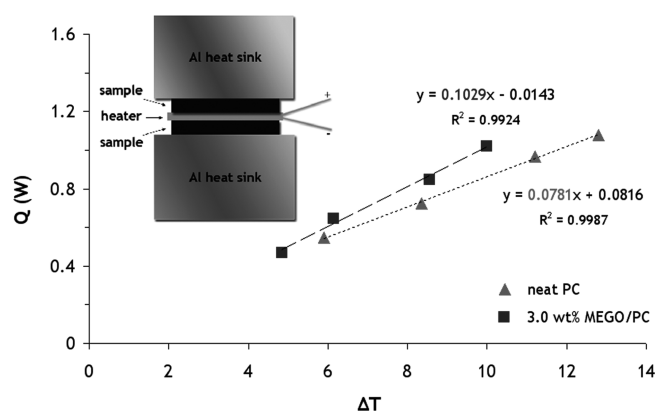
Figure 8. Data from thermal conductivity measurements on neat PC and MEGO/PC composites. Q represents the heat flow from the heater through the samples, while ΔT is the average temperature gradient across the two samples. The slope of the trendlines were taken as the thermal conductance, from which the thermal conductivity could be calculated for each loading tested. The inset schematic illustrates the construction of the "guarded hot plate" setup used to perform the measurements.

200 nm Brownian platelets in the PC matrix to be ~60 000 s at 230 °C and observed good experimental agreement in the modulus recovery with time, thus suggesting an appropriate time scale for annealing of MEGO/PC composites. Indeed, the electrical conductivities of the composite samples at 1.3 wt % and above were found to increase after a 24 h annealing treatment, as shown in Figure 7b. However, conductivity percolation was not observed at lower loadings following the annealing treatment (i.e., the resistances of the 0.8 and 0.5 wt % samples were still too high to be measured by our test setup), possibly because the concentration of platelets at these loadings is too low to form a percolated network, regardless of platelet orientation.

Above the conductivity percolation threshold, the electrical conductivity, σ, generally scales as a power law function:

$$\sigma \propto \sigma_0(\phi - \phi_c)^t$$

where ϕ is the volume fraction loading of MEGO, ϕ_c is the conductivity percolation threshold (volume fraction), σ_0 is the conductivity of the matrix, and t is a scaling exponent, which has been suggested to depend on the dimensionality of the system.[15,37] Fitting this expression to the data, as shown in Figure 7b with $\phi_c \sim 0.006$, suggests $t = 2.14$ for the as-molded composite samples and $t = 1.80$ for the 24 h-annealed samples. Both values of t are close to the value of 2 predicted by percolation theory for a three-dimensional conducting network.[38]

3.5. Thermal Conductivity and Thermal Stability. Pristine graphene has been reported to have a thermal conductivity as high as 5000 W/(m K),[39,40] and although no measurements have been reported to date on the thermal conductivity of GO-derived materials such as MEGO or reduced graphene oxide, it is expected that such materials may also exhibit high thermal conductivities—albeit much lower than pristine graphene due to the presence of defects and residual functional groups. There have been several reports on the use of graphite nanoplatelets to improve the thermal conductivity of polymers; however, to date, there have been few reports on the thermal conductivity of polymer

Table 2. Effect of Long-Term Thermal Annealing on the Electrical and Thermal Conductivity of MEGO/PC Composites

loading (wt %)	electrical conductivity (S/m)		thermal conductivity (W/(m K))	
	as-molded	annealed[a]	as-molded	annealed[b]
neat PC			0.19 ± 0.02	
0.5			0.18 ± 0.03	
1.3	2.2×10^{-5}	5.1×10^{-4}		
2.1	9.0×10^{-4}	5.0×10^{-3}	0.20 ± 0.03	0.22 ± 0.04
3.0	2.5×10^{-3}	0.036	0.23 ± 0.03	0.24 ± 0.02

[a] 24 h at 230 °C. [b] 14 h at 230 °C.

composites with GO-derived fillers, particularly with amorphous thermoplastic matrices such as PC.[1]

In this study, thermal conductivity measurements were made at steady-state using a "guarded hot plate" setup as described in section 2.9. According to a previous analysis, the total uncertainty in the measurements with this setup and sample geometry is ~6%.[18] A sample set of results are shown in Figure 8 for neat PC and a 3.0 wt % MEGO/PC composite. Taking the thermal conductance, G, from the slope of a plot of Q versus T, the thermal conductivity k was then calculated according to the equation

$$k = \frac{Gt}{2A}$$

where t is the sample thickness and A is the sample area. We measured the thermal conductivity of neat PC to be 0.19 ± 0.02 W/(m K), while for the 3.0 wt % MEGO/PC composite, a value of 0.23 ± 0.03 W/(m K) was obtained (see Table 2).

The improvement in thermal conductivity observed in this study is well below the upper bound predicted by a simple rule of mixtures;[41] despite the onset of electrical percolation around 1.3 wt % leading to large increases in electrical conductivity, only small increases in thermal conductivity were observed. Comparably small improvements in thermal conductivity have also been generally observed in carbon nanotube-filled composites,[41,42] although it is expected that graphene-based fillers could ultimately provide superior thermal conductivity enhancement due to lower interparticle thermal resistance.[43,44] However, relative to the large (many orders of magnitude) improvements observed in electrical conductivity, conductive fillers will generally provide much smaller improvements in thermal conductivity at equal loadings due to the considerably smaller contrast between the thermal conductivity of the polymer matrix and the filler, compared with the contrast in the electrical conductivity.[42]

Relative to the thin films pressed for electrical conductivity measurements, the 3 mm-thick samples pressed for thermal conductivity measurements may have had less flow-induced filler alignment and thus better filler connectivity.[13] Still, as our measurements were made transversely to the flow direction, we also sought to evaluate the effect of a long-term annealing treatment (as described in section 2.9) on the composites' thermal conductivity. However, as shown in Table 2, the annealing process was found to have little effect on the thermal conductivity of the composites, despite the significant increase observed in the electrical conductivity.
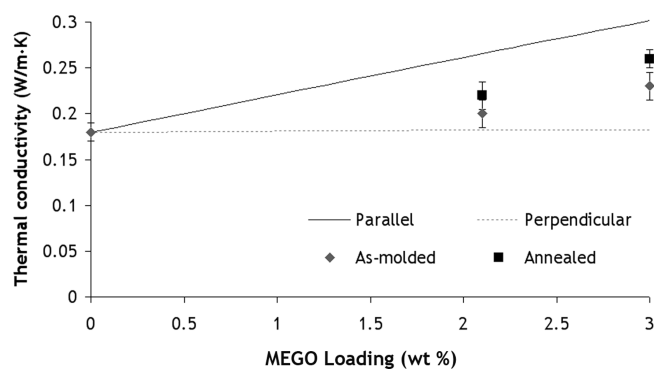
Figure 9. Comparison of thermal conductivity measurements to predictions of composite thermal conductivity from the Hatta and Taya model. "Parallel" represents the model prediction of the composite conductivity parallel to the plane of the aligned platelets, while "perpendicular" represents the conductivity out-of-plane. A filler thermal conductivity of 100 W/(m K) was used for the calculation, along with a matrix thermal conductivity of 0.19 W/(m K) and a platelet aspect ratio of 45.
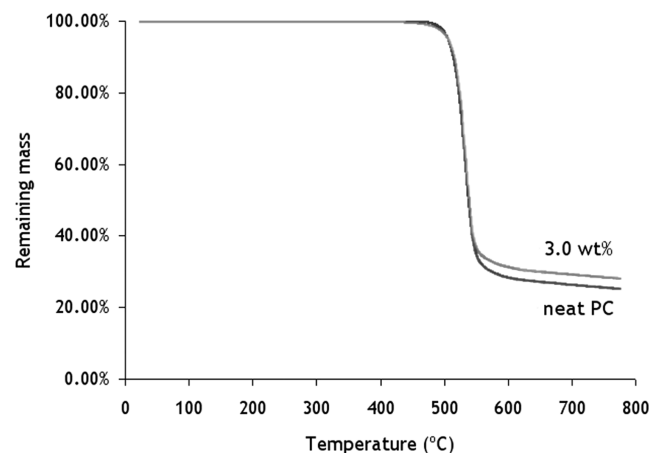

Figure 10. TGA plots of neat PC versus a 3.0 wt % MEGO/PC composite show a very small improvement in thermal stability of the composites relative to neat PC.

Improvements in thermal conductivity can be used as a measure of dispersion; several models for predicting the thermal conductivity of polymer composites exist.[45] The equivalent inclusion method developed by Hatta and Taya allows for estimation of composite thermal conductivity both parallel and perpendicular to the plane of aligned, disk-shaped platelets in a polymer matrix:[45,46]

$$k_c = k_m \left[1 + \frac{\phi}{S(1 - \phi) + k_m/(k_f - k_m)} \right]$$

where k_c, k_m, and k_f are the thermal conductivities of the composite, matrix, and filler particles, respectively, ϕ is the volume fraction of filler, and S is a shape factor that depends on A_f and orientation according to $S = \pi/4A_f$ for measurements parallel to the plane of orientation or $S = 1 - \pi/2A_f$ for measurements perpendicular to the plane of orientation. For an A_f of 45 (as estimated from TEM analysis), the composite thermal conductivity was found to be nearly independent of the

intrinsic platelet conductivity above 100 W/(m K), according to the model. Moreover, for any value of the filler conductivity greater than the matrix, the composite thermal conductivity at 3.0 wt % and A_f = 45 was calculated to be ~0.19 W/(m K) perpendicular to the plane of orientation, thus suggesting some level of disorientation in the as-molded composites (i.e., the dispersed platelets were oriented at some range of angles to the hot pressing direction) as suggested by Figure 9. While defects and residual functional groups in the structure of MEGO may limit its intrinsic thermal conductivity, our analysis suggests that the dispersion (i.e., A_f) might be the more important factor limiting the thermal conductivity of the composites,[47] particularly in light of recent work by Wang and co-workers reporting a 400% improvement in the thermal conductivity of a (unreduced) graphene oxide/epoxy composite at 5 wt %.[48]

Graphene-based fillers have been widely reported to improve the thermal stability of polymer composites relative to the host polymer.[1,2] Thermal degradation studies of the composites were performed using thermogravimetric analysis. The results are shown in Figure 10, where the shift in the onset of the thermal degradation temperature is plotted against loading of MEGO. Very little change in the nonoxidative thermal stability was observed with higher weight percent loadings of MEGO filler (data for other loadings not shown). Differences in the residual mass between composites of different loadings were used to assign "true" loading values, since some MEGO was lost during handling and particularly the mixing step.

4. CONCLUSIONS

The dispersion of MEGO into PC via melt mixing results in multifunctional property improvements versus neat PC. TEM images of the composites showed multilayer platelets well-dispersed throughout the PC matrix, with an average aspect ratio of ~45. Rheological measurements suggested an onset of connectivity percolation around 2.1 wt %, while electrical percolation was observed around 1.3 wt %, and long-term thermal annealing of the composites well above T_g was found to improve the electrical conductivity further. However, only modest increases in thermal conductivity were observed in this study. Moreover, the improvements in stiffness and conductivity came at the cost of diminished transparency and decreased impact strength. But despite these shortcomings, this study shows that MEGO can be easily dispersed into a suitable polymer matrix via melt compounding, while offering lower conductivity percolation thresholds and comparable electrical conductivity improvements to thermally exfoliated graphite oxide and multiwalled carbon nanotubes.[37] Moreover, the large electrical conductivity improvements coupled with the small thermal conductivity gains observed in this work suggests possible interesting new directions for graphene-based polymer composites, such as thermoelectrics.[49] Given the facile synthesis of MEGO, this approach described here may provide a highly attractive route to graphene-based polymer composites.

■ AUTHOR INFORMATION

Corresponding Author
*E-mail: r.ruoff@mail.utexas.edu.

Notes
§Visiting Scholar, Ruoff Laboratory.

■ REFERENCES

(1) Potts, J. R.; Dreyer, D. R.; Bielawski, C. W.; Ruoff, R. S. *Polymer* **2011**, *52* (1), 5–25.

(2) Kim, H.; Abdala, A. A.; Macosko, C. W. *Macromolecules* **2010**, *43* (16), 6515–6530.

(3) Dreyer, D. R.; Park, S.; Bielawski, C. W.; Ruoff, R. S. *Chem. Soc. Rev.* **2010**, *39* (1), 228–240.

(4) Park, S.; Ruoff, R. S. *Nature Nanotechnol.* **2009**, *4*, 217–224.

(5) Rourke, J. P.; Pandey, P. A.; Moore, J. J.; Bates, M.; Kinloch, I. A.; Young, R. J.; Wilson, N. R. *Angew. Chem.* **2011**, *123*, 3231–3235.

(6) Li, D.; Muller, M. B.; Gilje, S.; Kaner, R. B.; Wallace, G. G. *Nature Nanotechnol.* **2008**, *3* (2), 101–105.

(7) Stankovich, S.; Piner, R. D.; Chen, X.; Wu, N.; Nguyen, S. B. T.; Ruoff, R. S. *J. Mater. Chem.* **2006**, *16*, 155–158.

(8) Ruess, V. G.; Vogt, F. *Monatsh. Chem.* **1948**, *78*, 222–242.

(9) Schniepp, H. C.; Li, J. L.; McAllister, M. J.; Sai, H.; Herrera-Alonso, M.; Adamson, D. H.; Prud'homme, R. K.; Car, R.; Saville, D. A.; Aksay, I. A. *J. Phys. Chem. B* **2006**, *110* (17), 8535–8539.

(10) Zhu, Y. W.; Murali, S.; Stoller, M. D.; Velamakanni, A.; Piner, R. D.; Ruoff, R. S. *Carbon* **2010**, *48* (7), 2118–2122.

(11) Yoonessi, M.; Gaier, J. R. *ACS Nano* **2010**, *4* (12), 7211–7220.

(12) Kim, H.; Macosko, C. W. *Macromolecules* **2008**, *41* (9), 3317–3327.

(13) Kim, H.; Macosko, C. W. *Polymer* **2009**, *50* (15), 3797–3809.

(14) Kim, H.; Miura, Y.; Macosko, C. W. *Chem. Mater.* **2010**, *22* (11), 3441–3450.

(15) Zhang, H. B.; Zheng, W. G.; Yan, Q.; Yang, Y.; Wang, J. W.; Lu, Z. H.; Ji, G. Y.; Yu, Z. Z. *Polymer* **2010**, *51* (5), 1191–1196.

(16) Hummers, W. S.; Offeman, R. E. *J. Am. Chem. Soc.* **1958**, *80* (6), 1339.

(17) Brunauer, S.; Emmett, P. H.; Teller, E. *J. Am. Chem. Soc.* **1938**, *60* (2), 309–319.

(18) Moore, A. L.; Cummings, A. T.; Jensen, J. M.; Shi, L.; Koo, J. H. *J. Heat Transfer* **2009**, *131*, 091602.

(19) Paul, D. R.; Robeson, L. M. *Polymer* **2008**, *49* (15), 3187–3204.

(20) Vermant, J.; Ceccia, S.; Dolgovskij, M. K.; Maffettone, P. L.; Macosko, C. W. *J. Rheol.* **2007**, *51* (3), 429–450.

(21) Krishnamoorti, R.; Yurekli, K. *Curr. Opin. Colloid Interface Sci.* **2001**, *6*, 464–470.

(22) Ren, J.; Silva, A. S.; Krishnamoorti, R. *Macromolecules* **2000**, *33* (10), 3739–3746.

(23) Suk, J. W.; Piner, R. D.; An, J.; Ruoff, R. S. *ACS Nano* **2010**, *4* (11), 6557–6564.

(24) Gómez-Navarro, C.; Burghard, M.; Kern, K. *Nano Lett.* **2008**, *8* (7), 2045–2049.

(25) Fornes, T. D.; Paul, D. R. *Polymer* **2003**, *44* (17), 4993–5013.

(26) Zhao, X.; Zhang, Q. H.; Chen, D. J.; Lu, P. *Macromolecules* **2010**, *43* (5), 2357–2363.

(27) Mori, T.; Tanaka, K. *Acta Metall.* **1973**, *21*, 571–574.

(28) Tandon, G. P.; Weng, G. J. *Polym. Compos.* **1984**, *5*, 327–333.

(29) Brandrup, J.; Immergut, E. H.; Grulke, E. A.; Abe, A.; Bloch, D. R. *Polymer Handbook*, 4th ed.; John Wiley and Sons: New York, 1999; p 2336.

(30) Lee, C.; Wei, X.; Kysar, J. W.; Hone, J. *Science* **2008**, *321* (5887), 385–388.

(31) Brune, D. A.; Bicerano, J. *Polymer* **2002**, *43* (2), 369–387.

(32) Potts, J. R.; Lee, S. H.; Alam, T. M.; An, J.; Stoller, M. D.; Piner, R. D.; Ruoff, R. S. *Carbon* **2011**, *49*, 2615–2623.

(33) Hsieh, A. J.; Moy, P.; Beyer, F. L.; Madison, P.; Napadensky, E.; Ren, J.; Krishnamoorti, R. *Polym. Eng. Sci.* **2004**, *44* (5), 825–837.

(34) Yoon, P. J.; Hunter, D. L.; Paul, D. R. *Polymer* **2003**, *44* (18), 5323–5339.

(35) Steurer, P.; Wissert, R.; Thomann, R.; Mulhaupt, R. *Macromol. Rapid Commun.* **2009**, *30* (4−5), 316–327.

(36) Ren, J.; Casanueva, B. F.; Mitchell, C. A.; Krishnamoorti, R. *Macromolecules* **2003**, *36* (11), 4188–4194.

(37) Bauhofer, W.; Kovacs, J. Z. *Compos. Sci. Technol.* **2009**, *69* (10), 1486–1498.

(38) Kovacs, J. Z.; Velagala, B. S.; Schulte, K.; Bauhofer, W. *Compos. Sci. Technol.* **2007**, *67* (5), 922–928.

(39) Balandin, A. A.; Ghosh, S.; Bao, W.; Calizo, I.; Teweldebrhan, D.; Miao, F.; Lau, C. N. *Nano Lett.* **2008**, *8* (3), 902–907.

(40) Seol, J. H.; Jo, I.; Moore, A. L.; Lindsay, L.; Aitken, Z. H.; Pettes, M. T.; Li, X.; Yao, Z.; Huang, R.; Broido, D.; Mingo, N.; Ruoff, R. S.; Shi, L. *Science* **2010**, *328* (5975), 213–216.

(41) Han, Z.; Fina, A. *Prog. Polym. Sci.* **2011**, *36* (7), 914–944.

(42) Moniruzzaman, M.; Winey, K. I. *Macromolecules* **2006**, *39* (16), 5194–5205.

(43) Yu, A.; Ramesh, P.; Sun, X.; Bekyarova, E.; Itkis, M. E.; Haddon, R. C. *Adv. Mater.* **2008**, *20* (24), 4740–4744.

(44) Lin, W.; Zhang, R.; Wong, C. P. *J. Electron. Mater.* **2010**, *39* (3), 268–272.

(45) Hill, R. F.; Supancic, P. H. *J. Am. Ceram. Soc.* **2002**, *85* (4), 851–857.

(46) Hatta, H.; Taya, M. *Int. J. Eng. Sci.* **1986**, *24* (7), 1159–1170.

(47) Sun, X.; Ramesh, P.; Itkis, M. E.; Bekyarova, E.; Haddon, R. C. *J. Phys.: Condens. Matter* **2010**, *22* (33), 334216.

(48) Wang, S. R.; Tambraparni, M.; Qiu, J. J.; Tipton, J.; Dean, D. *Macromolecules* **2009**, *42* (14), 5251–5255.

(49) Choongho, Y.; Kim, Y. S.; Kim, D.; Grunlan, J. C. *Nano Lett.* **2008**, *8* (12), 4428–4432.

■ NOTE ADDED AFTER ASAP PUBLICATION

This manuscript was originally published on the web on July 27, 2011, with errors to the Abstract, Section 2, and Section 3. The corrected version was reposted on August 2, 2011.